Soft Matter

PAPER

View Article Online
View Journal | View Issue

Cite this: *Soft Matter*, 2017, **13**, 7514

Origin of spray formation during impact on heated surfaces

Michiel A. J. van Limbeek,[ab] Paul B. J. Hoefnagels,[a] Chao Sun[abc] and Detlef Lohse*[ab]

Received 12th May 2017,
Accepted 5th September 2017

DOI: 10.1039/c7sm00956a

rsc.li/soft-matter-journal

In many applications, it is crucial to control the heat transfer rate of impacting drops on a heated plate. When the solid exceeds the so-called Leidenfrost temperature, an impacting drop is prevented from contacting the plate by its own evaporation. But the decrease in the resulting cooling efficiency of the impacting drop is yet not quantitatively understood. Here, we experimentally study the impact of such water drops on smooth heated surfaces of various substances. We demonstrate that, in contrast to previous results for other liquids, water exhibits spray in the vertical direction when impacting sapphire and silicon. We show that this typical spray formation during impact is a result of the local cooling of the plate. This is surprising since these two materials were considered to remain isothermal during the impact of mm-sized droplets. We conclude and explain that the thermal time scale of the system is not solely determined by the thermal properties of the solid, but also by those of the liquid. We also introduce a dimensionless number comparing the thermal time scale and the dynamic time scale with which we can predict the spraying behaviour at impact.

1 Introduction

Many spray-cooling applications potentially risk the so-called burn-out phenomenon: at a certain temperature, the cooling efficiency drops significantly, potentially damaging expensive equipment or products. In this situation, direct contact between the solid and liquid is prevented by an insulating vapour layer, originating from the evaporating drop and separating it from the solid. The vapour film reduces the friction between the drop and the solid, resulting in an enhanced spreading behaviour[1,2] and fragmentation process.[3–6] The temperature at which this occurs is called the Leidenfrost temperature T_L[7–9] and depends on the thermo-physical properties of both the solid and the liquid, surface roughness and the impact velocity of the drop U,[6,10,11] where in context of the latter T_L is referred to as the dynamic Leidenfrost temperature. For obvious reasons, the prediction of T_L and the stability of the vapour film are of great importance.

For large-scale cooling applications, water is frequently used since it is omnipresent, inexpensive and has a large heat capacity. Therefore, it might not be surprising that the Leidenfrost phenomenon was first reported for water. By varying the ambient pressure, impact velocity, plate material, *etc.*,[12–17] many studies were focused on the prediction of the T_L. Most studies however make use of side-view observations, which are unable to image the liquid–solid interface, while it is at this interface, where heat is transferred between the drop and the plate.

The present study aims to unite and supplement the existing literature by studying the changes in the solid–liquid interface during the impact process for different velocities and plate temperatures, using the recent development of frustrated total internal reflection imaging (FTIR). This technique enables us to clearly discriminate between wetted areas with both high spatial and temporal resolutions. By identifying the various boiling regimes, we shed new light on the gradual change from contact boiling to Leidenfrost boiling. We will present the evidence of cooling effects on a sapphire plate, in contrast to previous claims of sapphire being isothermal.

2 Methods

Water drops were dispensed from a fine needle by a syringe pump from a height between 0.5 cm and 40 cm. Gravity and surface tension controlled the drop diameter D_0 at pinch off to be 3.8 mm and accelerated the drop to impact the plate with velocities U ranging from 0.3 m s^{-1} to 2.7 m s^{-1}. In most experiments, the plate was a sapphire right-angle prism (with side surfaces of (25 × 25) mm^2) of refractive index n = 1.76 placed in a

[a] *Physics of Fluids Group, Mesa+ Institute, University of Twente, 7500 AE Enschede, The Netherlands. E-mail: d.lohse@utwente.nl*
[b] *Max Planck Institute for Dynamics and Self-Organization, 37077 Göttingen, Germany*
[c] *Center for Combustion Energy and Department of Thermal Engineering, Tsinghua University, 100084 Beijing, China. E-mail: chaosun@tsinghua.edu.cn*

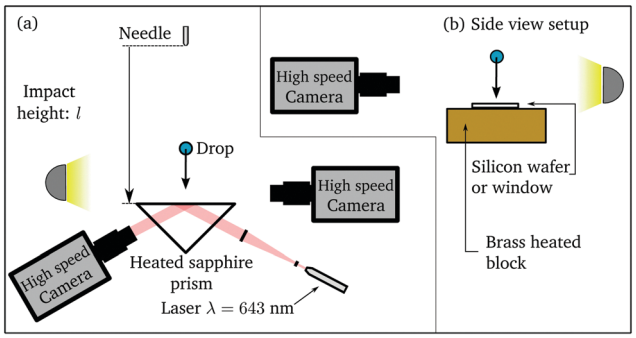

Fig. 1 Schematic of the two experimental setups used, depending on the plate material. In addition to the side-view observation, we employ in the case of the transparent sapphire prism (a) a measurement technique based on frustrated total internal reflection (FTIR) to study the liquid–solid interface. Since silicon is non-transparent to light, only a side view is possible (b).

aluminium heating block. The plate was kept at a constant temperature T_s by an electrical heater with a PID-control unit. For additional experiments, a silicon wafer of thickness 0.5 mm and another silicon plate of thickness 5 mm (ThorLabs WG81050 silicon window) were used for comparison with results from the existing literature. Prior to the impact, the top surface temperatures were measured by a surface probe. All impacts were recorded by a side-view camera (Photron Fascam APX) at 5000 fps, while the transparency of the sapphire prism also enabled the study of the liquid–solid interface using the bottom view. The technique used is based on frustrated total internal reflection (FTIR) imaging, where monochromatic parallel light (wavelength: 643 nm) is reflected internally on the rectangular phase of the prism, see Fig. 1 and ref. 18. The angle of incidence is chosen such that it exceeds the critical angle $\phi > \tan(1/n)^{-1}$. Wherever a drop touches the prism, the refractive index changes locally, enabling light to propagate into the drop, resulting in a black area on the camera allowing for a detailed study of dynamics present at the liquid–solid and liquid–vapour interfaces. The intermediate intensities correspond to the situation in which the drop is within one wavelength from the surface and can in principle be converted into an exact height map of the vapour film thickness (see ref. 18 and 19). To record the FTIR images, we used a high-speed camera (Photron Fastcam SA1.1) at 10 000 fps, equipped with a long-distance microscope (Navitar 12X Telecentric zoom system). Although both the prism and silicon surfaces have optically smooth surfaces, their thermal conductivity k_s differs significantly: 32 to 153 W m^{-1} K^{-1} respectively, reflected in a much higher thermal diffusivity $k_s/\rho C_p$ for the silicon plates (10^{-4} m^2 s^{-1}), compared to sapphire (10^{-5} m^2 s^{-1}), where ρ is the density and C_p the specific heat of the plate.

3 Results and discussion

A comparison of water drops of size D_0 impacting smooth silicon surfaces of different thicknesses can be seen in Fig. 2. Based on the criteria by Tran *et al.*,[16] such a spray shown in Fig. 2b indicates that the dynamic Leidenfrost temperature T_L

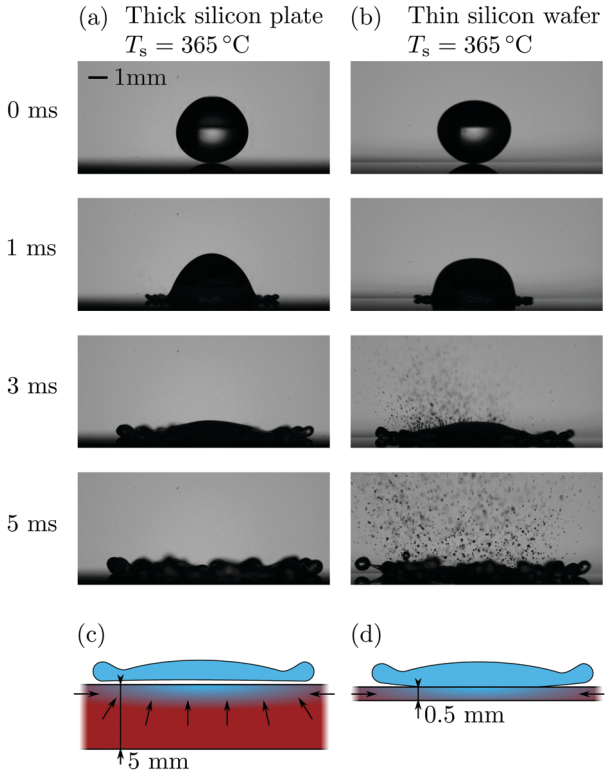

Fig. 2 Series of images of water drops impacting a silicon window of thickness 5 mm (a) and a 0.5 mm thick silicon wafer (b), initially at T = 365 °C at 1 m s^{-1}. The striking difference is the ejection of a droplet spray for the latter one, indicating an elevation in the Leidenfrost temperature (410 °C) for this system. In the sketches (c) and (d), the development of the thermal boundary layer is indicated in blue, where the arrows show the dominant heat fluxes. For a thin plate, only heat can be provided from the periphery of the impact area, while a thick window is able to also provide heat from below. The small shape deformations between the drops are a result of capillary waves originating from the pinch-off process when creating the drop.

has yet not been reached. We performed impacts on two silicon plates of different thicknesses, which are heated by a brass thermostat. The absence of the water spray in the case of a thick silicon window, shown in Fig. 2a, indicates that the finite plate thickness plays an important role for T_L here. Indeed, when estimating the thermal boundary layer δ_{th} developing inside the material, one finds it to be approximately $\sqrt{\frac{k_s}{\rho C_p}\frac{D_0}{U}} \approx 0.5$ mm, where we use the impact time scale $\tau = D_0/U$ as the typical exposure time for the surface for the cooling of the drop. Since this thermal boundary layer is of the same order as the thickness of the silicon wafer, we propose that during the impact, the cooling front penetrates through the thin wafer and as a consequence, the heat transport towards the top surface is reduced. Note that the roughness of the brass thermostat limits the replenishing rate of heat towards the silicon plates as isolating air is in between them. Hence, to keep a drop levitated, a higher T_L is expected for such plates. In the thick silicon plate on the other hand, being 5 mm thick, heat can still be transported from the bulk of the plate, keeping the

drop levitated during the full exposure time, see the sketches (c) and (d), resulting in a lower T_L.

The formation of spray during the impact of drops was also found when impacting ethanol drops on a glass plate. A direct comparison between impacts on glass and sapphire of similar smoothness (<10 nm) is presented in Fig. 3. It was found[10,20] that the difference in thermal conductivity caused the glass plate to cool down during the impact. Dendritic fingering structures of wetted areas with entrapped bubbles inside were observed in the case of glass[20,21] by frustrated total internal reflection (FTIR) imaging. Since the spray was only found in the case of cooling of the plate, it strengthens the suggestion that the spray in the present study in Fig. 2 is therefore also related

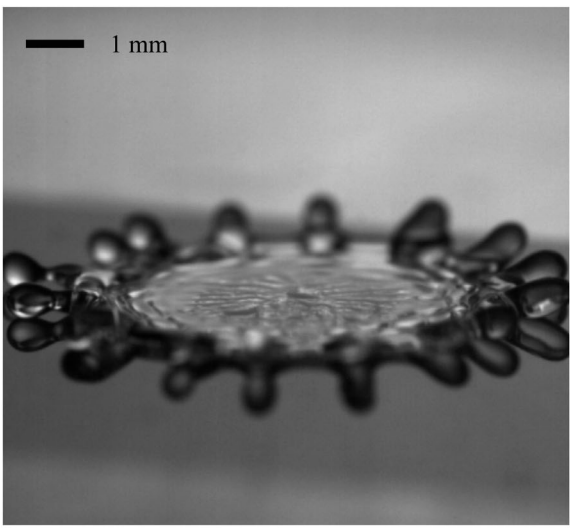

(a)

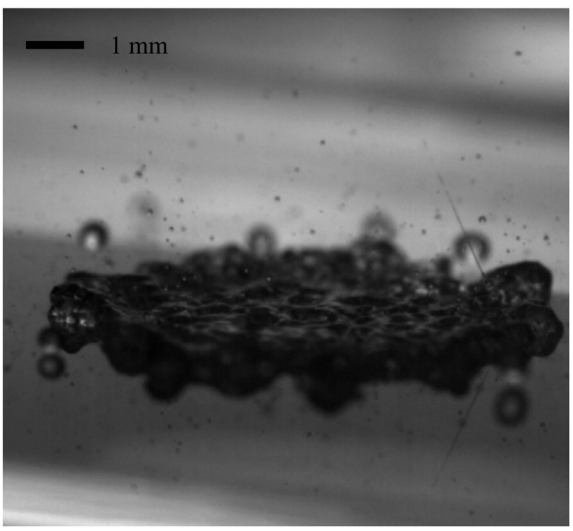

(b)

Fig. 3 Snapshots of ethanol drops taken at 6.5 ms after impacting a sapphire plate (a) and a glass plate (b), initially at a temperature of 200 °C and 207 °C, respectively. The presence of a spray in the latter correlates with the cooling of the plate. Note that this spray disturbs the top surface of the drop.

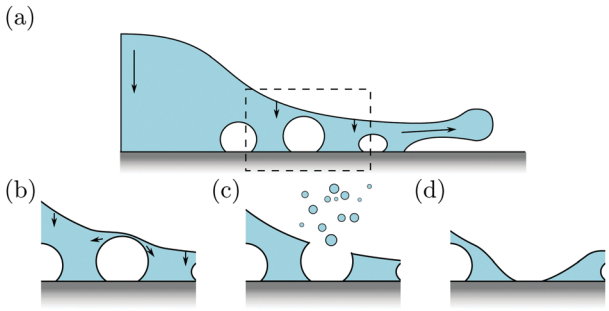

Fig. 4 Schematic of the bubble bursting mechanism. While the drop spreads as a result of the impact, the top of the drop approaches the bubble-covered wall (a). The drainage of the thin film at the top of the bubble (b) causes the bubble to burst, emitting a spray (c).[23] Further fragmentation of the drop can start from this location (d).

to the cooling of the solid. Cooling effects can therefore be observed by either a finite thickness of the plate or the plate lacking the ability to transport heat fast enough, originating from its low thermal diffusivity.

The spray observed is often related to the bursting of bubbles,[3,22,23] see the sketch in Fig. 4. Here, two mechanisms are considered to be of importance: the top surface of the drop should reach the bubble and therefore, a lower bound on the impact velocity can be expected. Secondly, the bubble should be a closed pocket, not connected to the surroundings.

To further understand how the cooling of the plate affects the dynamic Leidenfrost temperature of water, we employ a sapphire prism which, due to its transparency to light, enables us to study the wetting of the plate by the use of FTIR. This way, we can investigate the development of the solid–liquid interface and its dynamics over time.

3.1 Phase diagram

Using our FTIR measurements, we can discriminate the spreading radius R_s (*i.e.* the average radius enveloping all liquid of the drop) from the wetting radius R_w, which is the averaged radius of the solid–liquid contact line (see the sketches in Fig. 5), and study their behaviours over time. Based on this, three main regimes can be identified for the impact dynamics:[10] at low surface temperature, the drop is in direct contact with the surface, *i.e.* $R_s = R_w$, referred to as the contact boiling regime. Here, the full base of the drop thus wets the surface, while small isolated bubbles are nucleated on the wall.[10,12,17,24] At high temperature, no contact is observed, hence $R_w = 0$, called the Leidenfrost boiling regime. In between the transition, a boiling regime exists where partial touchdown is observed and $R_s > R_w$. Based on these classifications,[10,20] we obtain the phase diagram shown Fig. 5, together with the schematics of the different regimes. The phase diagram shows the observed boiling behaviour when varying the initial plate temperature T_s and impact velocity U. The shaded area represents conditions where a spray was observed by the side-view camera. With increasing temperature of the plate, more vapour is generated, until the Leidenfrost regime is reached. Since here no touchdown is observed, no bubbles are formed to pierce the flattening drop and release a spray by

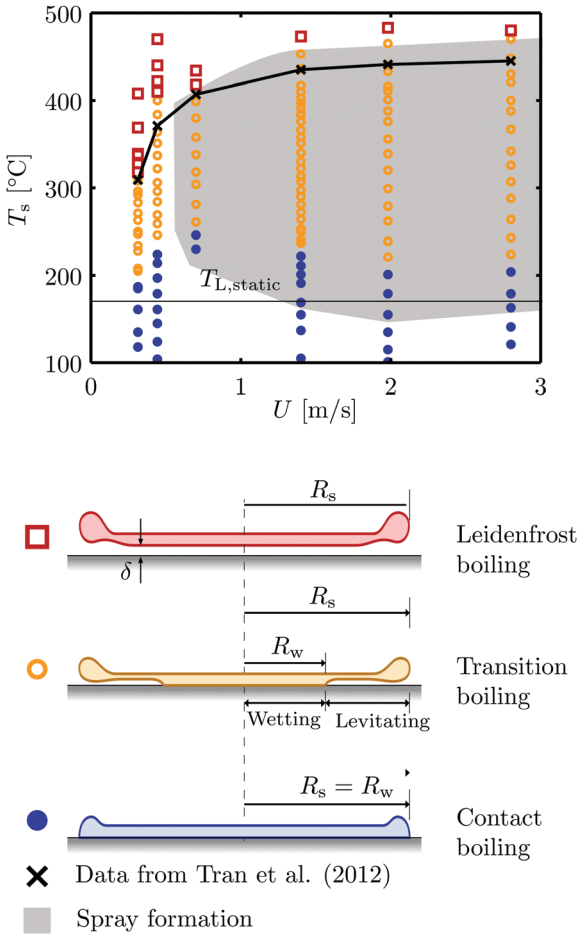

Fig. 5 Phase diagram of the observed boiling behaviours for water drops impacting a heated sapphire prism. Three regimes can be identified, based on the difference in wetting and spreading radii, see the sketches on the right. The shaded area denotes the conditions under which a vertical spray was observed.

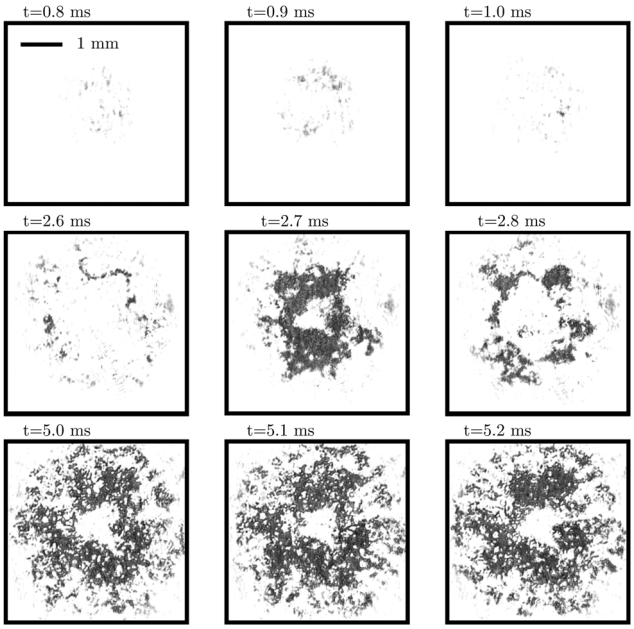

Fig. 6 Recordings of a water drop impacting a sapphire plate initially at T_s = 350 °C with a velocity U = 0.7 m s^{-1}. Three stages can be identified: first the drop is (temporary) in a Leidenfrost state (top row), as the drop is only visible in gray-scale.[18,19] This stage is succeeded by unstable boiling (middle row) where the drop touches the plate for a very short period. In the final stage, the drop is in a stable boiling state (bottom row) as the wetting pattern shows little change in time. The indicated time is the time after impact, as identified by the side-view camera. The displayed measurement corresponds to the point in the parameter space (Fig. 7) which is marked with a star.

bursting. Re-examination of the dataset reported by van Limbeek *et al.*[20] for ethanol drops impacting on glass (thickness of 1 mm) revealed the presence of a spray for all impacts in the transition boiling regime as well, though it was not observed for ethanol impacts on sapphire.

3.2 Cooling effect

A more in-depth analysis of the FTIR data reveals a variety of phenomena in the transition boiling regime, as shown in Fig. 6. Here, three different stages of the evaporative process are shown: over time, the drop is first levitated above the plate, similar to the Leidenfrost case. This situation however cannot be sustained and the drop begins to touch the plate at random locations for a short period of time, a state which is previously referred to as unstable boiling.[20] After a certain time after the drop impact, the cool-down time t_{cd}, some of these locations remain wetted for a long time as the plate is cooled down below the static Leidenfrost temperature,[20] referred to as stable boiling.

Whether or not all three phases are observed and at which time after the impact depends strongly on the plate temperature and impact velocity U of the drop. At low plate temperatures, only stable boiling is observed, previously identified as contact boiling + rim hovering.[20] The highest temperature at which contact is still observed only exhibits a change from Leidenfrost boiling into unstable boiling: due to the finite residence time of the drop near the plate, the plate cannot cool down enough to reach stable boiling. Since no cooling time can be observed, these measurements are not included in Fig. 8 and Section 3.3.

In between, the boiling changes from unstable to stable boiling or even through all three phases: from an initially Leidenfrost state *via* unstable boiling to stable boiling. One can expect the lowest plate temperature at which initially the drop remains separated from the plate (levitating) to be close to the dynamic Leidenfrost temperature T_L for an perfect thermal conducting solid. The characteristics on which we base our classification of the various (sub-) regimes are presented in Table 1. All states, except for the contact boiling + rim hovering state, are a result of the finite heat transfer rate through the solid towards the surface of the prism, referred to as vapour cooling.[20] The downward momentum forces the drop within a few hundred nanometers from the plate and the resulting heat flux consumed by the evaporation of the drop is large enough to locally cool the prism significantly.

Fig. 7 shows the inclusion of the two subregimes into the former phase diagram of Fig. 5, where the conditions exhibiting only stable boiling are represented by inverted triangles. The observed

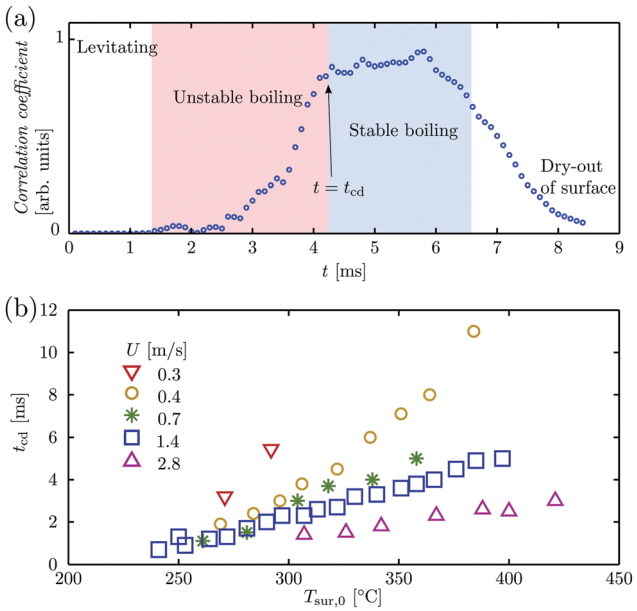

Fig. 8 Evolution of the correlation coefficient between two successive frames (a), corresponding to the measurement shown in Fig. 6. A low correlation is found while the drop is still hovering above the plate during the (temporary) Leidenfrost boiling. Once (brief) contact is established, the drop is in the unstable boiling state (indicated in red). The coefficient increases only slightly, while a sharp increase can be found when wetted patches remain for a long period on the surface (stable boiling, represented in blue). We define the cool-down time t_{cd} at the moment when the coefficient reaches its saturation, indicated by the arrow. Eventually, the drop boils away from the plate; the dry-out phase. In (b), we show the cool-down time t_{cd} for different impact velocities and initial plate temperatures.

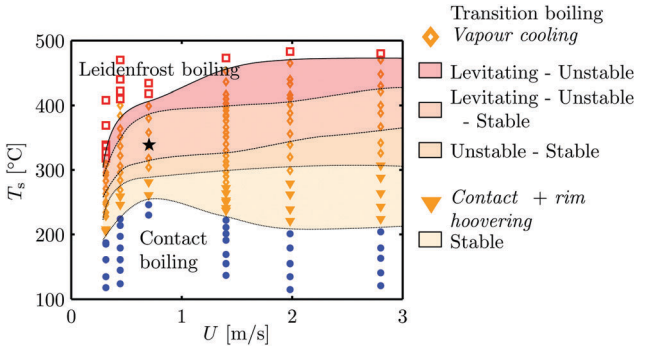

Fig. 7 Detailed phase diagram displaying the gradual change in boiling behaviour from contact to Leidenfrost boiling, indicated by the shaded areas. The FTIRimages of Fig. 6 correspond to the point in the parameter space which is marked with a star. Lines are a guide to the eye.

boiling regimes for the transition boiling regime are indicated by the shaded areas. Our observations for water however are in contrast to previous works using ethanol and FC-84 (C_7F_{16}) drops, where sapphire was shown by FTIR to remain isothermal during the impact.[10,20] A possible explanation might be the difference in enthalpy of vaporization, but from the current work it is yet unclear to make a conclusive explanation.

3.3 Thermal timescale

The cool down time t_{cd} can be measured using the correlation between two successive frames, see Fig. 8. Since we are interested in changes in intensity, we first subtract every frame from an image without an impact event. This image is also used to normalize all intensities. This way, the drop now appears gray against a black background, enhancing the signal to noise ratio. The correlation is expressed as the Frobenius inner product; *i.e.* $\langle I(t), I(t + \Delta t)\rangle_F = \sum I(t) \cdot I(t + \Delta t)$, where $\cdot$ is the Hadamard product for multiplication of the matrices and $\sum$ the sum over all pixels. The time Δt between the frames is in our recordings 100 μs.

In this example, the drop is initially only visible in gray values as the drop is not in direct contact with the plate and hence the correlation coefficient is almost zero. After 1.4 ms, the drop starts to touch the plate at random locations, but its rapid disappearance over time still results in a low coefficient. As a result of the cooling of the plate, from 3 ms onwards, the wetted areas tend to stabilize and the correlation between successive images increases. Once the correlation saturates, no rapid dewetting can be observed. The corresponding time, here 4.2 ms, is identified as the cool down time t_{cd}.

Using this method, we obtain t_{cd} at various initial plate temperatures and impact velocities, presented in Fig. 8(b). Two trends are clearly visible: first the cool-down time increases with increasing plate temperature, in agreement with previous results.[20] However, t_{cd} is found to strongly depend on U, decreasing with increasing impact velocity.

To quantify the cooling of the plate using our measurements of t_{cd}, we adopted the analysis method reported by van Limbeek *et al.*[20] to obtain the thermal time scale τ_{th} for the cooling in the plate. Since we have seen that t_{cd} depends on U, we expect that

Table 1 Overview of the different (sub-)regimes and boiling behaviours as classified from the FTIR observations

Observations				Classification		
$R_s = R_w$	Drop touches at $t \approx 0$	Drop touches any time	Wetted patches dewet rapidly between frames	Regime	Subregime	Boiling behaviour
Yes	Yes	Yes	No	Contact boiling	—	—
No	Yes	Yes	No	Transition boiling	Contact boiling + rim hovering	Stable boiling
No	Yes	Yes	Initially	Transition boiling	Vapour cooling	Unstable – stable boiling
No	No	Yes	Temporary, but delayed	Transition boiling	Vapour cooling	Levetating – unstable – stable boiling
No	No	Yes	Yes, but delayed	Transition boiling	Vapour cooling	Levitating – unstable boiling
No	No	No	No	Leidenfrost boiling	—	—

$\tau_{th}(U)$ and hence the analysis will be performed for every U separately. The separation of length scales between the vapour thickness and the drop radius justifies the use of a one-dimensional conduction model $\partial_t T = \frac{k_s}{\rho_s C_p}\partial_{xx} T$, where the plate of thermal conductivity k_s, density ρ_s and specific heat C_p are initially at $T = T_s$. The top surface of the plate is subject to the constant flux boundary condition $k_s \partial_x T|_{x=0} = \bar{h}(T_{sur} - T_{sat})$, where $\bar{h}$ (with units J s^{-1} K^{-1} m^{-2}) is the time-averaged heat transfer coefficient and $T_{sur} \equiv T(x = 0)$. The analytic solution to the problem is well known[13,24–26] and yields for the cooling of the top surface:

$$\frac{T_{sur}(t) - T_{sat}}{T_{sur,0} - T_{sat}} = \exp\left(\frac{t}{\tau_{th}}\right)\mathrm{erfc}\left(\sqrt{\frac{t}{\tau_{th}}}\right), \quad (1)$$

where $\tau_{th} = k\rho_s C_p \bar{h}^{-2}$. We have seen that at $t = t_{cd}$, the plate has cooled down to the static Leidenfrost temperature,[20] $T_{sur}(t = t_{cd}) = 170$ °C, which we measured separately. The remaining unknown τ_{th} can be obtained by solving eqn (1) implicitly:

$$\frac{T_{sur}(t_{cd}) - T_{sat}}{T_{sur,0} - T_{sat}} = \frac{170\ °C - 100\ °C}{T_{sur,0} - 100\ °C} = \exp\left(\frac{t_{cd}}{\tau_{th}}\right)\mathrm{erfc}\left(\sqrt{\frac{t_{cd}}{\tau_{th}}}\right). \quad (2)$$

By using measurements of t_{cd} for impacts at various initial plate temperatures, we increase the accuracy of τ_{th} by a fit as shown in Fig. 9a. Here, every symbol represents the measured t_{cd}, depending on $T_{sur,0}$ and grouped by impact velocity. The curves show eqn (2), using the thermal time scale τ_{th} as a fitting parameter. The impact velocity dependence of τ_{th} can be observed when plotting $\tau_{th}(U)$ (Fig. 9b), inversely scaling with U (inset). The velocity dependency of τ_{th} arises from the fact that, at higher impact velocities, the drop is more strongly forced onto the plate for early times.[27–29] Since $\bar{h} \approx \frac{1}{t}\int_0^t k_v \frac{\Delta T(\tilde{t})}{\delta(\tilde{t})} d\tilde{t}$, a higher initial forcing reduces the vapour layer thickness δ and hence decreases τ_{th}.

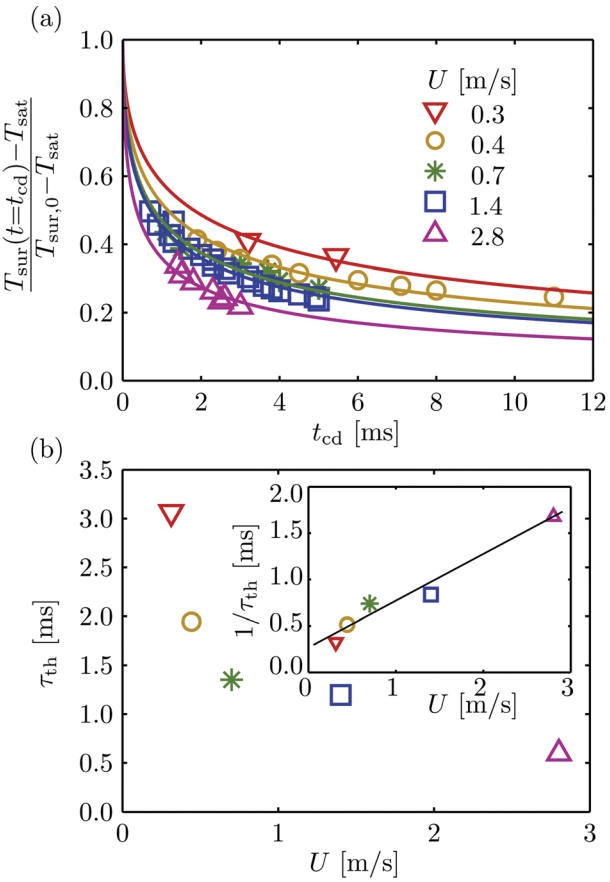

Fig. 9 The (non-dimensionalized) plate temperature decreases with time. At $t = t_{cd}$, the plate has cooled down to the static Leidenfrost temperature: $T_{sur}(t = t_{cd}) = 170$ °C. The data points are plotted in panel (a) for various initial plate temperatures $T_{sur,0}$ and impact velocities U representing separate experiments. By fitting eqn (1) (see the main text), the thermal time scale τ_{th} is obtained and presented in (b) as a function of the impact velocity. The inset reveals $\tau_{th}^{-1} \propto U$.

3.3.1 Exposure time to cooling. To quantify the significance of cooling, it is interesting to compare τ_{th} with the typical exposure time of the phenomenon. In the present case of an impacting drop, we therefore use the residence time of the drop near the plate, for which we consider the impact time scale $\tau = D_0/U$. For this ratio, we can define the following dimensionless number:

$$\Pi = \frac{\tau}{\tau_{th}}. \quad (3)$$

Two extremes can be addressed easily: for $\Pi \ll 1$, the plate remains isothermal during all stages of the impact process. This is usually the case for good thermal conducting materials. Shortly after the drop touchdown due to the high pressure zones arising from the impact, the wetted areas are boiled away and the drop becomes levitated for the remainder of the impact time. For $\Pi \gg 1$ however, the limitation in heat transfer lowers the surface temperature below the static Leidenfrost temperature[20] significantly. Even drops which remain levitated in the initial stages can touchdown eventually due to the insufficient heat transfer towards the drop interface. This is the case of solids of poor thermal conductivity or for plates of small thickness as we have seen in the case of a water drop impacting on a silicon wafer (Fig. 2b).

In the present case of water impacting on sapphire, we obtained for all impact velocities Π to be between 1.7 and 3, and found that τ_{th} has become a function of U itself. Since both time scales are comparable, it is not surprising that we observed a smooth transition from the contact boiling regime into the Leidenfrost regime with increasing initial plate temperature. It is expected that all stages are present for all situations where $\Pi \gg 1$, but the shorter the τ_{th}, the faster the various stages succeed one another. In these cases, to still observe them, the frame rate of the camera must allow for a good temporal resolution.

3.4 Reflection on the existing literature

If we compare our measurements with the results by Tran *et al.*,[16] we obtain a good agreement for the dynamic Leidenfrost temperature of water, see Fig. 5. This is surprising because the study by Tran *et al.* was expected to be on an isothermal plate. However, we found that the occurrence of a spray from side-view

observation strongly correlates with the presence of wetted areas with entrapped bubbles on the solid surface, as observed by FTIR. Since the surface cools down as a result of the presence of the drop, the wetted areas with their entrapped bubbles can survive on the surface, resulting in the spray formation by the bursting of the bubbles at the top surface of the drop, in agreement with previous studies on spray formation.[3,22] Both the present observation and the study by Tran *et al.* are subject to cooling, in which the first one is limited by the lower thermal conductivity of the plate and the latter study by the finite thickness of the plate. Furthermore, we find the boundary between contact boiling and transition boiling to be weakly dependent on the impact velocity, similarly to that reported for ethanol drops impacting on glass[20] and on sapphire.[5,10] Since no cooling was found in the latter two studies, it is not surprising that no spray is formed: the wetted area in the transition regime is boiled away long before the top interface of the drop has come close to the bubbles. Because of the absence of the spray, Staat *et al.*[5] identified all impacts above this boundary to be film boiling, though in later studies the lower part of this regime was named and identified as the transition boiling regime.[10,20]

4 Conclusion

Our study of water drops impacting on smooth surfaces has revealed that the presence of a spray is a signature of cooling effects in the plate. We have shown that water drops cool down the plate at a rate which depends on the impact velocity. Utilizing side-view imaging, we found that the dynamic Leidenfrost temperature was found only when the plate is subject to cooling as on a good thermal conductor, the wetted area from the impact boils away before bubbles can generate a spray by bursting at the top surface of the drop. Our study indicates that sapphire cannot always behave isothermally, as the difference in liquid properties could also play a fundamental role. This deserves more systematic studies in the future and we think that our new introduced dimensionless parameter Π, which compares the dynamical to the thermal time scale, is a useful tool for such an analysis.

Conflicts of interest

There are no conflicts of interest to declare.

Acknowledgements

The authors thank A. Prosperetti and M. Shirota for fruitful discussions. This work was supported by an ERC-Advanced Grant.

References

1 A.-L. Biance, F. Chevy, C. Clanet, G. Lagubeau and D. Quéré, *J. Fluid Mech.*, 2006, **554**, 47–66.
2 H. Lastakowski, F. Boyer, A.-L. Biance, C. Pirat and C. Ybert, *J. Fluid Mech.*, 2014, **747**, 103–118.
3 G. E. Cossali, M. Marengo and M. Santini, *Int. J. Heat Fluid Flow*, 2008, **29**, 167–177.
4 A.-L. Biance, C. Pirat and C. Ybert, *Phys. Fluids*, 2011, **23**, 022104.
5 H. J. J. Staat, T. Tran, B. Geerdink, G. Riboux, C. Sun, J. M. Gordillo and D. Lohse, *J. Fluid Mech.*, 2015, **779**, R3.
6 T. Tran, H. J. J. Staat, A. Susarrey-Arce, T. C. Foertsch, A. van Houselt, H. J. G. E. Gardeniers, A. Prosperetti, D. Lohse and C. Sun, *Soft Matter*, 2013, **9**, 3272–3282.
7 J. G. Leidenfrost, De aquae communis nonnullis qualitatibus tractatus, Ovenius, Duisburg, 1756.
8 A.-L. Biance, C. Clanet and D. Quéré, *Phys. Fluids*, 2003, **15**, 1632–1637.
9 D. Quéré, *Annu. Rev. Fluid Mech.*, 2013, **45**, 197–215.
10 M. Shirota, M. A. J. van Limbeek, C. Sun, A. Prosperetti and D. Lohse, *Phys. Rev. Lett.*, 2016, **116**, 064501.
11 H. Nair, H. J. J. Staat, T. Tran, A. van Houselt, A. Prosperetti, D. Lohse and C. Sun, *Soft Matter*, 2014, **10**, 2102–2109.
12 S. Chandra and C. T. Avedisian, *Proc. R. Soc. London, Ser. A*, 1991, **432**, 13–41.
13 K. J. Baumeister and F. F. Simon, *J. Heat Transfer*, 1973, **95**, 166–173.
14 G. S. Emmerson and C. W. Snoek, *Int. J. Heat and Mass Transfer*, 1978, **21**, 1081–1086.
15 D. Orejon, K. Sefiane and Y. Takata, *Phys. Rev. E: Stat., Nonlinear, Soft Matter Phys.*, 2014, **90**, 053012.
16 T. Tran, H. J. J. Staat, A. Prosperetti, C. Sun and D. Lohse, *Phys. Rev. Lett.*, 2012, **108**, 036101.
17 J. D. Bernardin, C. J. Stebbins and I. Mudawar, *Int. J. Heat Mass Transfer*, 1997, **40**, 247–267.
18 M. Shirota, M. A. van Limbeek, D. Lohse and C. Sun, *Eur. Phys. J. E: Soft Matter Biol. Phys.*, 2017, **40**, 54.
19 J. M. Kolinski, S. M. Rubinstein, S. Mandre, M. P. Brenner, D. A. Weitz and L. Mahadevan, *Phys. Rev. Lett.*, 2012, **108**, 074503.
20 M. A. J. van Limbeek, M. Shirota, P. Sleutel, C. Sun, A. Prosperetti and D. Lohse, *Int. J. Heat and Mass Transfer*, 2016, **97**, 101–109.
21 M. Khavari, C. Sun, D. Lohse and T. Tran, *Soft Matter*, 2015, **11**, 3298–3303.
22 H. Chaves, A. M. Kubitzek and F. Obermeier, *Int. J. Heat Fluid Flow*, 1999, **20**, 470–476.
23 G. Liger-Belair, G. Polidori and P. Jeandet, *Chem. Soc. Rev.*, 2008, **37**, 2490–2511.
24 Y. M. Qiao and S. Chandra, *Int. J. Heat and Mass Transfer*, 1996, **39**, 1379–1393.
25 H. S. Carslaw and J. C. Jaeger, *Conduction of heat in solids*, Clarendon Press, Oxford, 2nd edn, 1959.
26 A. Bejan, *Heat Transfer*, John Wiley@Sons, Inc., New York, 1st edn, 1993.
27 J. Philippi, P.-Y. Lagrée and A. Antkowiak, *J. Fluid Mech.*, 2016, **795**, 96–135.
28 J. Eggers, M. A. Fontelos, C. Josserand and S. Zaleski, *Phys. Fluids*, 2010, **22**, 062101.
29 W. Bouwhuis, R. C. A. van der Veen, T. Tran, D. L. Keij, K. G. Winkels, I. R. Peters, D. van der Meer, C. Sun, J. H. Snoeijer and D. Lohse, *Phys. Rev. Lett.*, 2012, **109**, 264501.